ARCHIVES OF ELECTRICAL ENGINEERING VOL. X(Y), pp. 1-20 (2027)

This paper has been accepted for publication in the AEE journal. This is the version, which has not been fully edited and content may change prior to final publication.
Citation information: DOI 10.24425/aee.2027.11175

Induced voltage prediction in transmission line parameter testing based on hyperparameter optimized Set-Transformer

PENG CHANG*, LIANGLIANG SONG, CHENQING WANG

Electric Power Research Institute, State Grid Jiangsu Electric Power Co., Ltd.
Nanjing 211103, China
*e-mail:*292945750@qq.com, {songliang1005/wcqmorning}@163.com*

Early Access

Abstract: The analysis and prediction of induced voltages in transmission lines are of great significance for ensuring the safety of line operation and maintenance. To address the varying coupling effects caused by electromagnetic environment non-uniformity in non-fully parallel lines, a novel prediction method based on an improved Set Transformer is proposed. First, a feature set characterizing line-induced voltages is extracted through theoretical analysis based on historical test data. Hyperparameters of the Set Transformer are then optimized by the Optuna optimizer, and an Optuna-ST based prediction model is established for both electrostatically and electromagnetically induced voltages. The model is trained and tested on the collected samples, and its effectiveness is further validated through field case studies. The results show that the Optuna-ST model can achieve a Normalized Mean Absolute Error (NMAE) of about 6%, a Tolerance accuracy above 85%, and a coefficient of determination (R^2) exceeding 0.98. The model can accurately predict induced voltages between non-fully parallel transmission lines. Compared with representative baselines such as Convolutional Neural Network (CNN) and Light Gradient Boosting Machine (LightGBM), this method has higher prediction accuracy, reliability, and generalization capability, providing a crucial decision-making basis for ensuring safety during line parameter testing.

Keywords: induced voltage prediction, hyperparameter optimization, non-parallel transmission lines, set transformer

1. Introduction

With the continuous expansion of power systems and the rapid acceleration of urbanization, transmission line corridor resources have become increasingly scarce [1–3]. To improve corridor utilization, transmission lines are often arranged in corridors, segmented parallel paths, or crossing configurations, with over 60% of high-voltage lines only sharing corridors on a part of the entire route [4–5]. Unlike lines erected on the same tower along the full length, non-fully parallel lines experience electromagnetic coupling only over specific sections, resulting in significant spatial disparities in the electromagnetic environment and complex induced voltage

This paper has been accepted for publication in the AEE journal. This is the version, which has not been fully edited and content may change prior to final publication.
Citation information: DOI 10.24425/aee.2027.11175

distribution [6]. These excessive induced voltages pose severe threats to personnel safety and equipment reliability during field maintenance. For personnel safety, according to GB/T 3805-2008 and IEEE Std 1048-2016, the steady-state safe touch voltage threshold for the human body under normal dry conditions is 50 V (reduced to 25 V in damp outdoor environments). Once this threshold is exceeded, the resulting body current rapidly surpasses the human let-go threshold (10 mA, IEC 60479-1:2018), generating fatal electric shock hazards during the installation and removal of portable protective grounds. In field measurements, steady-state induced voltages on de-energized lines have reached hundreds of volts (such as 322.3 V on Line A and 95.2 V on Line B), far exceeding safe physiological limits. For equipment protection, excessive induced currents can easily excess the rated making and breaking capacity of substation earthing switches (GB/T 1985-2023/IEC 62271-102:2018), causing strong reignition and thermal contact erosion. In addition, strong electromagnetic coupling threatens the front-end circuit of the line parameter tester by exceeding its input overvoltage withstand capability (DL/T 1119-2010/DL/T 1583-2016), which may lead to dielectric breakdown or instrument burnout. Consequently, the rapid and high-precision prediction of induced voltages in non-fully parallel corridors before maintenance and testing is an essential prerequisite for verifying safety margins and assessing the necessity of deploying auxiliary damping and suppression devices.

Existing studies on induced voltage calculation have mainly focused on multi-circuit transmission lines on the same tower. Wang *et al.* [7] performed a detailed investigation of the electromagnetic and electrostatic coupling between ±500 kV MMC-HVDC and 500 kV AC lines on the same tower, and proposed corresponding improvement schemes for protective relaying. This approach successfully identified the risk of relay mal-operation and system interruption under cross-line faults. Chen *et al.* [8] established a systematic simulation and analysis method on the EMTP/ATP platform using a multi-transmission line model to investigate the power-frequency induced voltage in 35 kV OPGW systems. This method successfully revealed key characteristics such as the "V-shaped" voltage distribution, the proportionality to load current, and the significant impact of double-circuit phase sequence, thereby providing critical insights for the safe design and application of OPGW in new power systems. Zhang *et al.* [9] quantitatively analyzed the electromagnetic coupling of UHV AC and DC parallel lines. It pointed out that the resulting steady-state induced voltage is within safe limits and does not affect the effectiveness of the operating methods and tools established in current maintenance procedures. Wu *et al.* [10] used the Deutsch assumption and empirical formula to calculate multiple electromagnetic environment indicators of ±800 kV and ±500 kV double-circuit DC lines on the same tower under different structural parameters. The results can provide quantitative data support for the engineering design of such transmission lines. The methods for calculating induced voltage are mainly divided into two categories: numerical simulation and two-dimensional analytical models. Although numerical simulation can accurately characterize complex electromagnetic environments, it involves cumbersome modeling procedures. Conversely, although 2D analytical models have high computational efficiency, their accuracy is limited when dealing with complex line structures such as non-perfectly parallel lines. Both

Early Access

This paper has been accepted for publication in the AEE journal. This is the version, which has not been fully edited and content may change prior to final publication.
Citation information: DOI 10.24425/aee.2027.11175

methods struggle to achieve efficient and accurate characterization of electromagnetic coupling mechanisms in 3D spatial configurations, leaving a clear methodological gap that must be addressed.

To address these limitations, artificial intelligence and data-driven methods have recently been introduced into electromagnetic computation for transmission lines [11–13]. Karami *et al*. [11] deployed deep learning to invert lightning-induced voltages and localize lightning sources; Li *et al*. [12] integrated heuristic optimization with the charge simulation method to analyze electric fields beneath UHV lines; Lu *et al*. [13] developed a genetic algorithm-optimized backpropagation neural network (GA-BPNN) to predict induction parameters of 500 kV multi-circuit lines, demonstrating the feasibility of surrogate models in replacing burdensome numerical simulations under fixed tower geometries. However, when generalized to multi-body scenarios in non-fully parallel corridors, existing machine learning architectures have three fundamental physical and structural mismatches:

1) Contradiction between dimensional rigidity and dynamic circuit cardinality: Standard models such as MLP and SVR mandate fixed-dimension input vectors. In practical corridors, the number of adjacent energized circuits fluctuates dynamically (typically 1 to 4 circuits) and conventional models mainly rely on zero-padding. This introduces a virtual conductor with zero coordinates and zero current, which distorts the spatial feature distribution and injects stray electromagnetic coupling bias [14];

2) Conflict between permutation variance and electromagnetic superposition symmetry: Physically, adjacent energized circuits from a disordered excitation source mush strictly follow the permutation invariance-permutation of the input indices of any two circuits and generate the same induced voltage on the target line. Conventional networks, however, treat inputs as ordered vectors and must resort on N! factorial data augmentation to learn order-invariance (a strategy that inflates sample complexity and poses severe overfitting risks on scarce field test datasets) [15];

3) Mismatch of spatial inductive bias: The Euclidean grid translation invariance of CNNs (Convolutional Neural Networks) and the causal sequential assumptions of RNNs (Recurrent Neural Networks) fundamentally contradict the instantaneous 3D spatial superposition of Maxwellian electromagnetic fields. Flattening continuous geometric attributes such as crossing angles (θ), non-uniform spans and phase clearances fails to capture the continuous multi-body nonlinear spatial interactions of non-parallel corridors [16].

To fundamentally resolve these structural limitations, this study proposes an induced voltage prediction framework tailored to non-fully parallel transmission corridors based on an improved Set Transformer (ST). First, an expressive spatial and electrical feature set is extracted through theoretical analysis of electromagnetic and electrostatic coupling mechanisms. Then, by adopting a dual-stream permutation-invariant architecture equipped with dynamic attention masking, the proposed model seamlessly accommodates variable line cardinalities (1 to 4 circuits) without zero-padding distortion while strictly preserving the permutation invariance of unordered field sources. In addition, the Tree-structured Parzen Estimator (TPE) algorithm within the Optuna framework is integrated to automatically optimize the network

Early Access

This paper has been accepted for publication in the AEE journal. This is the version, which has not been fully edited and content may change prior to final publication.
Citation information: DOI 10.24425/aee.2027.11175

hyperparameters. Field case studies demonstrate that this Optuna-ST framework achieves high prediction accuracy, robust generalization, and millisecond-level inference speed under different and unaligned line configurations.

2. Analysis of electromagnetic interference sources in line measurement

2.1. Theoretical analysis of induced voltage

The induced voltage between transmission lines mainly includes electromagnetically and electrostatically induced voltages [17–18]. When one line is out of service and the other is in operation, the operating line can induce a voltage on the adjacent out-of-service line through electrostatic and magnetic coupling [19–21].

Taking phase *a* of the out-of-service line in Fig. 1 as an example, the traditional method for calculating induced voltage is introduced:

1) The electrostatically induced voltage is mainly determined by the operating line voltage and the spatial geometric relationship between the lines. The calculation formula is as follows:

$$U_1 = U_2 = \frac{C_{Aa}U_A + C_{Ba}U_B + C_{Ca}U_C}{C_{Aa} + C_{Ba} + C_{Ca} + C_0}. \tag{1}$$

2) The electromagnetically induced voltage is mainly determined by the operating line current and the spatial geometric relationship between the lines. The calculation formula is as follows:

$$U_1 \approx |\omega l(M_{Aa}I_A + M_{Ba}I_B + M_{Ca}I_C)|, \tag{2}$$

where C_{Aa}, C_{Ba}, and C_{Ca} are the mutual capacitances between each phase of the normally operating Line ABC and the phase *a* of the out-of-service line, respectively; M_{Aa}, M_{Ba}, and M_{Ca} are the mutual inductances between each phase of the normally operating Line ABC and the phase *a* of the out-of-service line, respectively; C_0 is the capacitance to ground of the out-of-service line; U_A, U_B, and U_C are the operating voltages of each phase of the normally operating Line ABC; I_A, I_B, and I_C are the operating currents of each phase of the normally operating Line ABC [22–23].

Early Access

This paper has been accepted for publication in the AEE journal. This is the version, which has not been fully edited and content may change prior to final publication.
Citation information: DOI 10.24425/aee.2027.11175

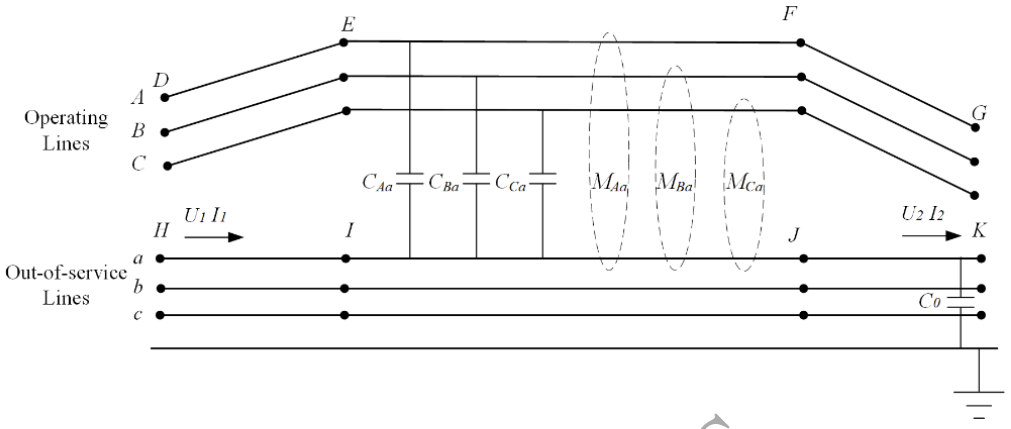


Fig. 1. Model diagram of non-fully parallel lines

However, traditional methods rely on the ideal assumptions of parallel lines and a uniform electromagnetic environment, and simplify the 3D model to a 2D model for calculation. Under such simplifications, parameters such as mutual capacitance and mutual inductance in the calculation formulas become independent of the location of the line. This simplification cannot address the problem of non-uniform parameter distribution caused by segmentation, crossings, and terrain undulations. Therefore, it is necessary to construct a model that accurately reflects the 3D spatial topology and solves for the dynamically changing electromagnetic coupling parameters based on spatial location, replacing the traditional parameter assumptions.

Early Access

2.2. Feature analysis

Based on historical test data and theoretical analysis, the electrostatically induced voltage is mainly related to factors such as line operating voltage, parallel section length, and line spacing; electromagnetically induced voltage is related to factors such as line operating current, parallel section length, line spacing, and ground loop characteristics. When lines cross each other, the electromagnetic coupling effect between them weakens as the angle increases. In the case of multiple parallel lines, the total induced voltage is the vector sum of the induced effects of each operating line, and its superposition effect depends on the phase relationship between them.

Through the above theoretical analysis of induced voltage, a set of features characterizing the electromagnetic coupling parameters of lines are extracted. For an out-of-service line, its own geometric features include length, height, and conductor radius. When the number of operating lines is denoted by n, each adjacent energized line has six features: length, height, voltage, current, parallel spacing, and angle. Therefore, the total number of features can be expressed as $3 + 6n$. The factors affecting induced voltage are classified as shown in Table 1.

Table 1. Classification of factors affecting induced voltage

Type	Influencing factors

This paper has been accepted for publication in the AEE journal. This is the version, which has not been fully edited and content may change prior to final publication.
Citation information: DOI 10.24425/aee.2027.11175

Line structure parameters	Tower spacing, split conductor information, line transposition method, conductor model, ground wire model, etc.
Line geometry parameters	Relevant distances between phase conductors, line height parameters, line length parameters, reference outer diameter, angle, etc.
Line electrical parameters	Voltage level, line flow, etc.
Other parameters	Soil resistivity, grounding method, etc.

In the Set-Transformer architecture, a hierarchical encoding strategy is used to project the fixed-dimensional features of the out-of-service line into a high-dimensional feature space. The electrical and geometric parameters of each operating line are independently encoded into a unified dimension, constructing a set representation matrix of operating lines. The Learnable Position Encoding (LPE) is introduced to distinguish the identities of individual lines. The Set Attention Blocks (SABs) are then utilized to achieve deep feature interactions of the lines, and a masking mechanism is incorporated to adaptively handle variable numbers of operating lines. The Pooling by Multi-head Attention (PMA) mechanism is applied to extract set-level global representations, where learnable seed vectors adaptively aggregate critical information from multiple lines, generating feature vectors that encapsulate aggregated multi-line information. Finally, through concatenating the fixed system encoding with the operating-line set encoding, a joint representation that integrates the global system state is formed. Consequently, the original multi-source heterogeneous raw features are transformed into a unified deep representation, providing a robust and discriminative input for subsequent prediction.

Early Access

3. Induced voltage prediction model based on SET-Transformer

3.1. Set-Transformer model theory

The Set-Transformer is a neural network architecture designed for set-structured data, which leverages self-attention mechanisms to achieve permutation invariance while effectively capturing complex interdependencies in elements. From a physical perspective, the total steady-state induced voltage on a target line is the instantaneous superposition of capacitive and inductive field excitations from all adjacent operating circuits. This physical result is strictly invariant to the indexing or sorting of adjacent lines, satisfying permutation invariance:

$$f(\{L_1, L_2, \dots, L_N\}) = f(\{L_{\pi(1)}, L_{\pi(2)}, \dots, L_{\pi(N)}\}), \tag{3}$$

where: L_i denotes the feature representation vector of the i-th adjacent operating circuit; N is the total number of adjacent operating circuits; $f(\cdot)$ denotes the nonlinear mapping function from the operating circuit set to the induced voltage on the target line, and π denotes an arbitrary permutation of the circuit index set $\{1, 2, ..., N\}$. Consequently, this architecture is mathematically and structurally well-suited for addressing multi-line non-fully-parallel corridors characterized by dynamic circuit counts (N) and unordered spatial topologies.

This paper has been accepted for publication in the AEE journal. This is the version, which has not been fully edited and content may change prior to final publication.
Citation information: DOI 10.24425/aee.2027.11175

The overall workflow of Set-Transformer for regression tasks includes the following key steps:

The learnable position encoding adds learnable positional to each element in the input set, enhancing the model capability to model relationships between elements and obtaining a position-aware set representation:

$$X_\text{encoded} = X + P\ \left(P \in R^{n\times d}\right), \tag{4}$$

where: X is the original input set matrix; P is the learnable position encoding matrix; X_encoded is the position-aware set representation; n is the number of elements in the set, and d is the feature dimension of each element.

The position-aware set representation is processed through multiple stacked set attention blocks. These blocks use a hierarchical attention mechanism to fully simulate complex interactions between set elements, yielding a deeply-interacted set feature representation:

$$H^{(0)} = X_\text{encoded}, \tag{5}$$

$$H^{(l)} = \text{SAB}\left(H^{(l-1)}\right)\ (l = 1,\ldots,L), \tag{6}$$

$$\text{SAB}(H) = \text{LayerNorm}\left(H'' + \text{FFN}(H'')\right), \tag{7}$$

$$H'' = \text{LayerNorm}\left(H + \text{MultiHeadAttention}(H,H,H)\right), \tag{8}$$

where $H^{(l)}$ is the set representation at layer l; L is the number of stacked Set Attention Block (SAB) layers; FFN is the Feed-forward Network; LayerNorm is the layer normalization operation, and MultiHeadAttention is the standard multi-head attention mechanism.

The deeply-interacted set feature representation is aggregated into a fixed-dimensional global representation through the pooling by Multi-head Attention Module. This module adaptively selects and weights critical information via learnable seed vectors, yielding a global feature vector that encapsulates aggregated multi-line information:

$$h_\text{global} = \text{PMA}\left(H^{(L)}\right), \tag{9}$$

$$\text{PMA}(H) = \text{MAB}(S,H)\ (S \in R^{1\times d}), \tag{10}$$

$$\text{MAB}(Q,K) = \text{LayerNorm}\left(H' + \text{FFN}(H')\right), \tag{11}$$

$$H' = \text{LayerNorm}\left(Q + \text{MultiHeadAttention}(Q,K,K)\right), \tag{12}$$

where: $H^{(L)}$ is the deeply-interacted set feature representation from the final SAB layer; h_global is the aggregated global feature vector; MAB is the Multi-head Attention Block; S is the learnable seed vectors; Q is the query matrix in attention mechanism, and K is the key matrix in attention mechanism.

The global feature vector is connected to the fixed system encoding to form a joint representation that integrates the global system state. This combination represents the use of a

Early Access

This paper has been accepted for publication in the AEE journal. This is the version, which has not been fully edited and content may change prior to final publication.
Citation information: DOI 10.24425/aee.2027.11175

Multi-layer Perceptron (MLP) output layer for nonlinear transformation, ultimately generating regression predictions for specific tasks:

$$h_\text{combined} = \text{Concat}(h_\text{fixed}, h_\text{global}), \tag{13}$$

$$y = \text{MLP}(h_\text{combined}), \tag{14}$$

where: h_fixed is the encoded fixed system feature representation; h_combined is the connected joint feature vector, and Concat denotes the connection operation along the feature dimension.

This architecture ensures permutation invariance for unordered sets. It can efficiently model complex set relationships through attention mechanisms and learnable components. The method has significant advantages in tasks that rely on set-structured data, including particle physics and multi-line coupled induced voltage prediction in power systems.

3.2. Optuna hyperparameter optimization

To address these limitations of conventional optimization methods, the Optuna hyperparameter optimization framework based on the Tree-structured Parzen Estimator(TPE) is established to perform automatic hyperparameter tuning for the Set Transformer model. A high-dimensional and heterogeneous hyperparameter space is introduced by the multi-head attention mechanism and set encoding structure of the Set Transformer. The sequential sampling strategy of Optuna can efficiently explore this complex space, and dynamic resource allocation and parallel-trial coordination achieve an effective balance between exploration and exploitation. Moreover, Optuna provides seamless integration with the PyTorch deep learning framework supports immediate feedback during training iterations, and implements adaptive early stopping for optimization. Collectively, these capabilities effectively alleviate gradient instability and overfitting issues encountered during Set Transformer training.

Early Access

The TPE algorithm adopts a hierarchical probabilistic model and non-parametric density estimation techniques. Specifically, the TPE first constructs probability model of the parameters by learning from historical evaluation results, and then identifies the optimal hyperparameter combination according to the relative impact of each parameter on the objective function. The specific procedure is described as follows:

Completed trials are first ranked by their corresponding loss values, y_i. The top γ quantile of these trials is defined as the good performance set, denoted as D_{good}. The remaining trials constitute the poor performance set, denoted as D_{bad}. This process is formally expressed as:

$$\begin{aligned} D_{\text{good}} &= \{(\theta_i, y_i) | y_i \le y^*\}, \\ D_{\text{bad}} &= \{(\theta_i, y_i) | y_i > y^*\}, \end{aligned} \tag{15}$$

where y^* is the threshold value corresponding to the γ-th quantile.

Probability density models are constructed for the sets D_{good} and D_{bad}, respectively:

$$l(\theta) = p(\theta | y \le y^*) = \frac{1}{|D_{\text{good}}|} \sum_{(\theta_i, y_i) \in D_{\text{good}}} K(\theta, \theta_i), \tag{16}$$

This paper has been accepted for publication in the AEE journal. This is the version, which has not been fully edited and content may change prior to final publication.
Citation information: DOI 10.24425/aee.2027.11175

$$g(\theta) = p(\theta|y > y^*) = \frac{1}{|D_{\text{bad}}|}\sum_{(\theta_i,y_i)\in D_{\text{bad}}} K(\theta,\theta_i), \tag{17}$$

where K is the Gaussian kernel function.

The improvement ratio, denoted as $r(\theta)$, is calculated as follows:

$$r(\theta) = \frac{l(\theta)}{g(\theta)}. \tag{18}$$

A set of candidate parameters is first sampled from the good distribution, $l(\theta)$. The parameter $r(\theta)$ that maximizes the improvement ratio is then selected from this candidate set:

$$\theta_{\text{new}} = \arg\max_{\theta} r(\theta). \tag{19}$$

In the hyperparameter optimization of the voltage prediction model, an efficient search in the high-dimensional, mixed parameter space is achieved. This is accomplished by the TPE-based Optuna framework based on non-parametric density estimation and a hierarchical probabilistic model, ensuring the performance enhancement of the Set Transformer model.

3.3. Model prediction process

The procedure for predicting induced voltages between non-fully parallel transmission lines based on Optuna-ST is shown in Fig. 2. The specific steps are as follows:

1) Data preprocessing and feature encoding

Valid operating line features are first identified for each data sample, and a masking mechanism dynamically is applied to flexibly accommodate variable numbers of operating lines. The six-dimensional features of each operating line are then independently encoded, and positional encoding is incorporated to preserve order-related information. Subsequently, the fixed features of the de-energized target line and the operating-line features are nonlinearly transformed through separate encoders, achieving a unified mapping in the feature space.

2) Data segmentation and standardization

The defined parameters have different physical meanings and exhibit significant heterogeneity in dimensions and magnitudes of different feature quantities. Direct model input will result in gradient descent dominated by high-value features. Therefore, before model training, standardize each feature dimension using (20).

$$z = \frac{x-\mu}{\sigma}, \tag{20}$$

where: μ is the mean value of the feature in the training set; x is the original feature value; z is the standardized feature value, and σ is the standard deviation of the feature in the training set.

3) Model assessment

The evaluation of the induced voltage prediction model for non-fully parallel transmission lines constitutes a crucial validation step. To comprehensively assess the model, five core evaluation metrics: Root Mean Square Error (RMSE), Mean Absolute Error (MAE), Normalized Mean Absolute Error (NMAE), coefficient of determination (R^2), and tolerance accuracy, are applied. These metrics collectively reflect the accuracy and effectiveness of the model from

Early Access

This paper has been accepted for publication in the AEE journal. This is the version, which has not been fully edited and content may change prior to final publication.
Citation information: DOI 10.24425/aee.2027.11175

different perspectives. In this study, tolerance accuracy is defined as the proportion of samples where predictions fall within the ±10% tolerance interval of the corresponding measured values. This metric effectively balances prediction errors of different magnitudes and provides a more engineering-relevant measure of the practical acceptability of prediction results in engineering applications.

$$\mathrm{MAE} = \frac{1}{n}\sum_{i=1}^{n}|y_i - \hat{y}_i|, \tag{21}$$

$$\mathrm{RMSE} = \sqrt{\frac{1}{n}\sum_{i=1}^{n}(y_i - \hat{y}_i)^2}, \tag{22}$$

$$\mathrm{NMAE} = 100\%\,\frac{\mathrm{MAE}}{\bar{y}}, \tag{23}$$

$$R^2 = 1 - \frac{\sum_{i=1}^{n}(y_i - \hat{y}_i)^2}{\sum_{i=1}^{n}(y_i - \bar{y})^2}, \tag{24}$$

where: y_i is the i-th measured induced voltage value; $\hat{y}_i$ is the corresponding model predicted value, and $\bar{y}$ is the sample mean of the measured induced voltage values.

Early Access

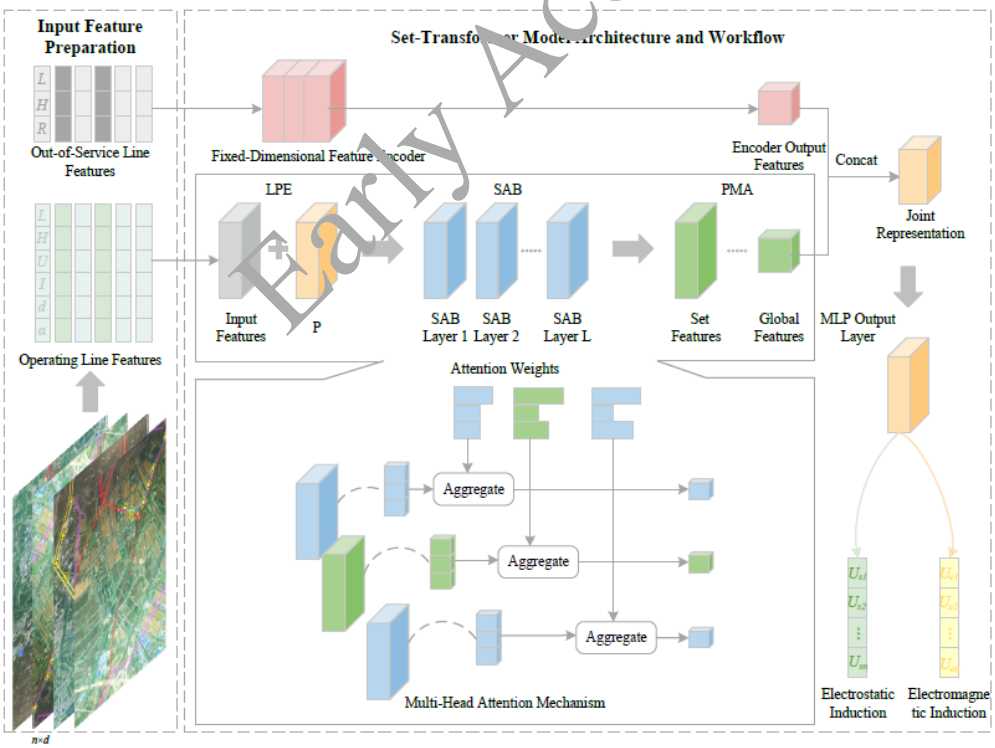


Fig. 2. Prediction process of induced voltage between non-full parallel transmission lines based on Optuna-ST

This paper has been accepted for publication in the AEE journal. This is the version, which has not been fully edited and content may change prior to final publication.
Citation information: DOI 10.24425/aee.2027.11175

4. Analysis of Optuna-ST model performance

A dataset consisting of 500 valid test records was constructed based on the actual on-site line parameter testing archives of the high-voltage transmission corridor in East China. The dataset captures different real-world electromagnetic environments, including different numbers of operating 500 kV and 220 kV circuits coexisting with de-energized target lines. The input features are divided into:

(i) – geometric attributes of the out-of-service line, and

(ii) – a spatial set of geometric and electrical parameters characterizing each adjacent operating line.

The detailed parameter definitions, units, types, and exact statistical ranges are shown in Table 2. These 500 samples were randomly divided into training (70%), validation (15%), and independent testing (15%) subsets. In addition, all continuous variables were standardized using z-score normalization before training.

Early Access

Table 2. Statistical ranges and characteristics of the line dataset

Parameters	Features	Symbols	Units	Types	Range/discrete values	Mean ± std
Out-of-service lines	Line length	L_0	km	Continuous	5.0 – 85.0	32.4 ± 18.2
	Conductor height	H	m	Continuous	12.0 – 38.0	22.5 ± 5.4
	Conductor radius	r_0	mm	Discrete	10.5, 13.4, 15.2, 16.8	—
Operating lines (Set)	Number of operating circuits	N	—	Discrete	1 – 4	2.1 ± 0.8
	Rated voltage level	U_n	kV	Discrete	220, 500	—
	Operating load current	I	A	Continuous	150 – 2400	820.5 ± 410.2
	Conductor height	H	m	Continuous	15.0 – 45.0	26.8 ± 6.1
	Horizontal line spacing	D	m	Continuous	15.0 – 120.0	42.6 ± 21.5
	Crossing/intersection angle	θ	deg (°)	Continuous	0 – 90	18.5 ± 22.3
Target outputs	Electrostatic induced voltage	U_s	V	Target	18.5 – 680.0	192.4 ± 115.6
	Electromagnetic induced voltage	U_m	V	Target	12.0 – 210.0	68.2 ± 42.1

This paper has been accepted for publication in the AEE journal. This is the version, which has not been fully edited and content may change prior to final publication.
Citation information: DOI 10.24425/aee.2027.11175

4.1. Hyperparameter values

The Set-Transformer model is centered around the Transformer encoder. Its parameter optimization is categorized into two main aspects: the one includes the key Transformer parameters that determine the model architecture, and the other involves the optimization parameters that control the training process. The key model hyperparameters are shown in Table 3.

Table 3. Key parameters of the Set-Transformer model

Parameters	Parameter meaning	Optimal parameters	Fixed parameters
*d*_model	Model dimension	512	256
num_heads	Number of attention heads	8	8
num_layers	Number of transformer layers	4	4
num_mlp_layers	Number of MLP layers	4	2
mlp_dropout	MLP dropout rate	0.26381	0.15
dropout	General dropout rate	0.10070	0.15
ffn_multiplier	Feed-forward Network multiplier	3	2
lr	Learning rate	0.00015	0.001

Early Access

In the Set-Transformer model, the parameter "*d*_model" defines the dimensionality of the internal representations of the model and serves as the benchmark for the width of all sub-layer outputs. "num_heads" determines the number of parallel working "heads" in the multi-head attention mechanism, enabling the model to focus on different aspects of the input at the same time. "num_layers" sets the number of stacked Transformer encoder blocks, directly influencing the depth and complexity of the model. Following these, "num_mlp_layers" specifically specifies the depth of the final output MLP, and "ffn_multiplier" controls the scaling factor of the hidden layer dimension relative to "*d*_model" in the Feed-forward Network. To prevent overfitting, "dropout" serves as a general regularization technique applied throughout the model, whereas "mlp_dropout" refers specifically to the dropout rate used in the final MLP. During training, "lr", as one of the most critical hyperparameters, controls the step size of parameter updates. The optimization path of the Set-Transformer hyperparameters is shown in Fig. 3. The horizontal axis shows the sequence of hyperparameters and the final objective-function value, and the vertical axis indicates the value space of each parameter. Each polyline corresponds to a full hyperparameter experiment, and its color gradient intuitively encoding the performance of the experiment. Influential hyperparameters can be recognized by examining the distribution patterns of these polylines. Through the guided fine-search process described above, the optimal hyperparameter configuration for the Set-Transformer was ultimately determined, as shown in Table 3.

This paper has been accepted for publication in the AEE journal. This is the version, which has not been fully edited and content may change prior to final publication.
Citation information: DOI 10.24425/aee.2027.11175

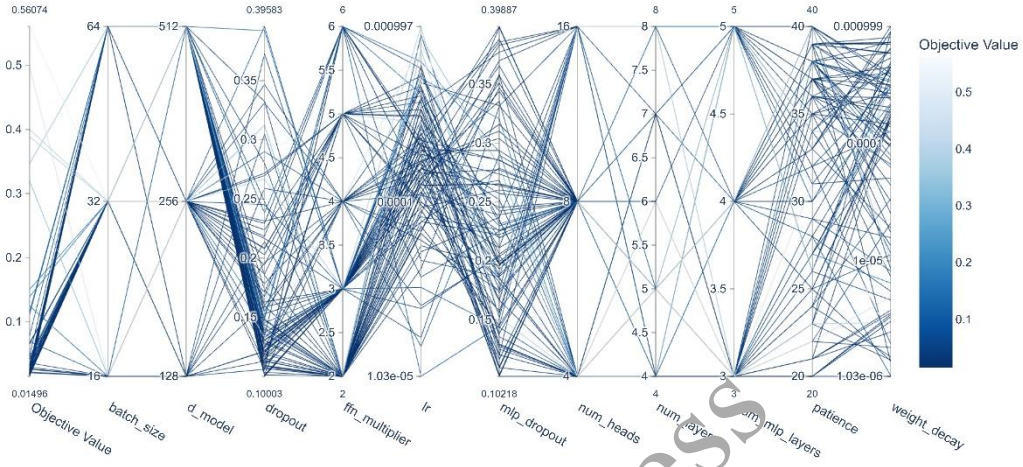
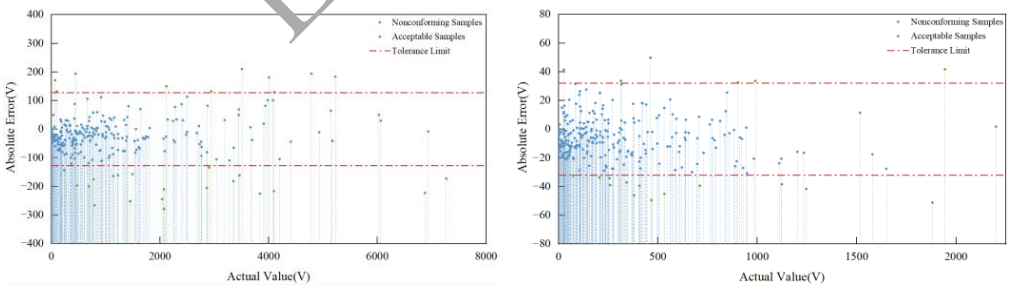


Fig. 3. Hyperparameter optimization parallel coordinates

4.2. Prediction results analysis

The effectiveness of the Optuna-ST model was validated. The prediction error distributions for the electrostatically and electromagnetically induced voltages are shown in Fig. 4 and Fig. 5, respectively. The analysis of the absolute error distribution indicates that the prediction errors of the model for both voltage types are highly concentrated near the zero-error line. Specifically, 85.7% of the electrostatically induced voltage samples and 90.9% of the electromagnetically induced voltage samples have errors in the tolerance band. These results validate the excellent accuracy and stability of the Optuna-ST model in both prediction tasks.

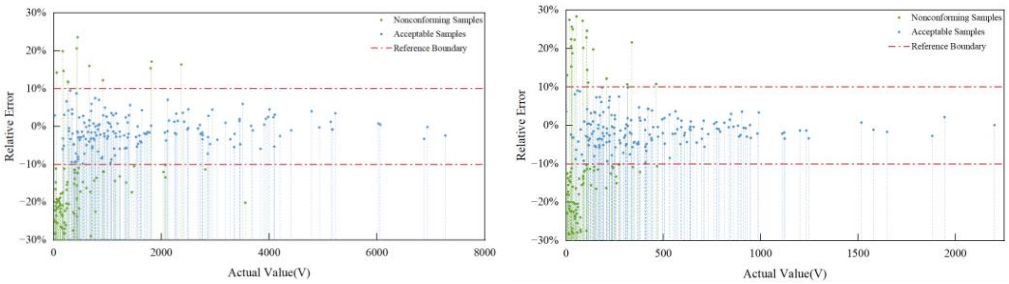
Early Access



(a) Electrostatically induced voltage (b) Electromagnetically induced voltage

Fig. 4. Absolute error distribution of Optuna-ST model results

This paper has been accepted for publication in the AEE journal. This is the version, which has not been fully edited and content may change prior to final publication.
Citation information: DOI 10.24425/aee.2027.11175



(a) Electrostatically induced voltage (b) Electromagnetically induced voltage

Fig. 5. Relative error distribution of Optuna-ST model results

To further evaluate the robustness of the model, the distribution of the relative error is shown in Fig. 5. It can be observed that there is significant dispersion of the relative error in small actual values due to the denominator effect. However, as the actual value increases, the relative error rapidly converges, and then becomes stably near the zero baseline. This demonstrates excellent consistency of the prediction.

To validate the effectiveness of the Optuna hyperparameter optimization framework for complex multi-objective tasks, a comparative analysis with a fixed-hyperparameter ST model was performed. As shown in Table 4, the Optuna-ST model significantly outperforms the baseline ST model in all key metrics. For electrostatically induced-voltage prediction, the Optuna-ST model achieves an 8.6% reduction in RMSE and 37.8% in MAE, demonstrating significant improvement in prediction error. The tolerance accuracy was improved by 18.8%, indicating a substantial enhancement in prediction precision and error control. For electromagnetically induced voltage prediction, the performance is even more significant: the RMSE is further reduced by 26.5%, the MAE is decreased by 42.1% and the tolerance accuracy is improved by 25.0%, indicating high prediction precision and error control capability. In both prediction tasks, R^2 is brought closer to 1, confirming stronger explanatory power for data variance and its ability to more accurately capture variation patterns of induced voltage.

Early Access

Table 4. Quantitative evaluation of induced voltage prediction results

Models	Sources	RMSE	MAE	NMAE	R^2	Accuracy
Optuna-ST	Electrostatic induction	225.2 V	92.0 V	6.5%	0.98	85.7%
	Electromagnetic induction	35.5 V	18.4 V	5.2%	0.99	90.9%
ST	Electrostatic induction	246.4 V	148 V	10.6%	0.97	66.9%
	Electromagnetic induction	48.3 V	31.8 V	9.1%	0.97	65.9%

This paper has been accepted for publication in the AEE journal. This is the version, which has not been fully edited and content may change prior to final publication.
Citation information: DOI 10.24425/aee.2027.11175

4.3. Comparison of prediction performance by algorithms

To validate the prediction performance of the Optuna-ST model, it is compared with the Convolutional Neural Network (CNN) and Light Gradient Boosting Machine (LightGBM).

To ensure the prediction performance of the model, automated hyperparameters are optimized before training by the Optuna framework. The hyperparameters of the CNN and LightGBM models are tuned to obtain optimal configurations of the dataset. The resulting key parameter values are shown in Table 5 and Table 6.

Table 5. Key parameters of the CNN model

Parameter name	Parameter meaning	Optimal parameters
conv_channel_0	Output channels of the first convolutional layer	64
conv_channel_1	Output channels of the second convolutional layer	128
kernel_size_0	Kernel size of the first convolutional layer	3
kernel_size_1	Kernel size of the second convolutional layer	3
mlp_layer_0	Number of neurons in the first fully-connected layer	128
mlp_layer_1	Number of neurons in the second fully-connected layer	512

Table 6. Key parameters of the LightGBM model for electrostatic voltage prediction

Parameters	Parameter meaning	Optimal parameters
num_leaves	Number of leaves in one tree	30
feature_fraction	Fraction of features to use for each iteration	0.93164
bagging_fraction	Fraction of data to use for each bagging	0.63370
bagging_freq	Frequency for bagging	5
min_child_samples	Minimal number of data in one leaf	14

Early Access

To objectively evaluate the performance differences between models in the induced voltage prediction task, Optuna-ST, Optuna-CNN, and Optuna-LightGBM are compared using multiple evaluation metrics. The data in Table 7 indicates a significant advantage of the Optuna-ST model. This performance is consistent in both electrostatically and electromagnetically induced voltage prediction.

In electrostatically induced voltage prediction, compared with Optuna-CNN, a reduction of 39.5% in RMSE was achieved by the Optuna-ST model. When compared with Optuna-LightGBM, the reduction can reach 11.9%. The MAE value is only 41.8% by Optuna-CNN, and maintains at 73.0% by the Optuna-LightGBM. For electromagnetically induced voltage prediction, the RMSE is further reduced by 45.2% and 39.6% compared to these two models respectively. The MAE values were only 43.7% and 61.5% of those benchmarks for the two

This paper has been accepted for publication in the AEE journal. This is the version, which has not been fully edited and content may change prior to final publication.
Citation information: DOI 10.24425/aee.2027.11175

prediction tasks, demonstrating particularly notable improvements in error control capability. The tolerance accuracy is excellent, with accuracies of 85.7% and 90.9% for electrostatic and electromagnetic predictions, respectively, confirming a higher proportion of predictions falling in acceptable engineering error margins. Regarding generalization capability, R^2 is maintained stably above 0.98 in both prediction tasks, and that of Optuna-CNN and Optuna-LightGBM for electrostatic prediction are 0.94 and 0.97 respectively. This further demonstrates the higher data-fitting and pattern-capture capability of the Optuna-ST model than conventional machine-learning baselines.

Table 7**.** Quantitative evaluation of induced voltage prediction results based on different algorithms

Models	Sources	RMSE	MAE	NMAE	R^2	Accuracy
Optuna-ST	Electrostatic induction	225.2 V	92.0 V	6.5%	0.98	85.7%
	Electromagnetic induction	35.5 V	18.4 V	5.2%	0.99	90.9%
Optuna-CNN	Electrostatic induction	372.4 V	220 V	15.7%	0.94	48.4%
	Electromagnetic induction	64.8 V	42.1 V	12.1%	0.97	50.3%
Optuna-LightGBM	Electrostatic induction	255.7 V	126 V	9.0%	0.97	77.6%
	Electromagnetic induction	58.8 V	29.9 V	8.6%	0.97	78.2%

Early Access

5. Case study

A 500 kV power transmission and transformation project was selected as a typical case to verify the on-site accuracy and engineering applicability of the proposed model. Combined with conventional line parameter testing, field measurements of induced voltage were conducted on 500 kV Line A and Line B. Infield testing, electrostatically and electromagnetically induced voltages were recorded for the two de-energized circuits under adjacent operating lines. For Line A, the measured electrostatically and electromagnetically induced voltages were 322.3 V and 90.1 V, respectively. For Line B, the corresponding measured values were 95.2 V and 76.5 V. To quantitatively evaluate the performance and error level of traditional calculation methods, the conventional two-dimensional analytical method based on Eqs. (1)–(2) and the proposed Optuna-ST model were implemented using the collected spatial and electrical parameters at the same time.

The predicted results from the proposed model and the calculated results from the traditional analytical method, as well as their relative errors and field measurements, are shown in Table 8. As shown in the comparative data, the traditional analytical method exhibits significant prediction errors on both lines: for Line A, the relative error for electrostatically induced voltage (calculated 270.8 V) reaches 1.98%, and for electromagnetically induced voltage (calculated 71.2 V) reaches 20.98%; for Line B, the corresponding errors reach 17.65% (calculated 78.4 V)

This paper has been accepted for publication in the AEE journal. This is the version, which has not been fully edited and content may change prior to final publication.
Citation information: DOI 10.24425/aee.2027.11175

and 21.18% (calculated 60.3 V), respectively. This significant difference is mainly due to the idealized assumption of infinite-parallel conductor in traditional analytical formulas. It neglects spatial crossing angles (θ) and non-uniform line clearances, leading to a systematic underestimation of actual induced voltage. In sharp contrast, the Optuna-ST model achieves a higher predictive accuracy in all scenarios: for Line A, the prediction errors are only 0.94% for electrostatically induced voltage (predicted 319.26 V) and 1.75% for electromagnetically induced voltage (predicted 88.52 V); for Line B, the errors remain well-controlled at 5.17% (predicted 100.12 V) and 5.41% (predicted 72.36 V), respectively. By effectively capturing the complex multi-body spatial coupling in non-parallel corridors, the proposed model reduces the error level from over 20% to within 5.5%, verifying its high fidelity and practical reliability in real-world engineering parameter testing.

Table 8. Comparison of measured and predicted induced voltages across different transmission lines

Types	Methods/values	Line A	Line B
Electrostatically induced voltage	Measured value	322.3 V	95.2 V
	Traditional analytical method	270.3 V	78.4 V
	Error of traditional method	15.98%	17.65%
	Proposed Optuna-ST	319.26 V	100.12 V
	Error of proposed method	0.94%	5.17%
Electromagnetically induced voltage	Measured value	90.1 V	76.5 V
	Traditional analytical method	71.2 V	60.3 V
	Error of traditional method	20.98%	21.18%
	Proposed Optuna-ST	88.52 V	72.36 V
	Error of proposed method	1.75%	5.41%

Early Access

6. Conclusion

A novel prediction method for line-induced voltage is proposed to address the varying coupling effects caused by electromagnetic environment non-uniformity in non-fully parallel lines. Based on comparative analysis and field validation, the following conclusions are drawn:

1) The Optuna ST model has shown excellent performance in predicting electrostatic and electromagnetic induced voltages. The NMAE remains at around 6%, and the tolerance accuracy is always above 85%, maintaining stable performance in complex scenarios. These include non-parallel configurations and cross spans. R^2 remains stable above 0.98. The results represent

This paper has been accepted for publication in the AEE journal. This is the version, which has not been fully edited and content may change prior to final publication.
Citation information: DOI 10.24425/aee.2027.11175

significant advantages over representative machine-learning algorithms such as convolutional neural networks (CNNs) and LightGBM, confirming the superior prediction accuracy, robustness, and generalization capability of the proposed framework;

2) The prediction performance is significantly improved through the Optuna hyperparameter optimization framework. Compared with the unoptimized baseline, the MAE of the optimized Set Transformer model is reduced by about 40%; the tolerance accuracy is improved by an average of 22%, and the R^2 is closer to 1. These quantitative achievements collectively demonstrate the enhanced fitting capability and stability of the optimized model, confirming the essential role of hyperparameter optimization in unlocking the full potential of the Set Transformer architecture for induced-voltage prediction.

3) The practical applicability of the model is further verified through typical engineering case studies. In all investigated scenarios, the prediction errors remain consistently below 6%, and the error distribution closely follows the patterns identified in the validation experiments, confirming the successful transition from theoretical framework to practical application. These results effectively demonstrate the reliability and generalization capability of the model under realistic operating conditions.

This study establishes a novel prediction methodology that effectively characterizes the complex spatial topologies of non-fully parallel transmission corridors, providing a robust technical foundation for accurate induced-voltage assessment and for the formulation of targeted protection measures. The proposed approach is therefore of critical importance for ensuring the safety of both maintenance personnel and electrical equipment during on-site line-parameter testing. Future work will focus on extending the proposed Optuna-ST framework to additional high-voltage corridors through transfer learning and integrating it with physics-based electromagnetic simulation to enhance generalization capability and interpretability for complex line configurations.

Early Access

Acknowledges

This research was funded by the Science and Technology Project of State Grid Jiangsu Electric Power Co., Ltd., contract number J2025147.

References

[1] Chen H., Hu Z., Wang Z., Tan J., Xu X., Sun Z., *New method for live line measuring the zero-sequence distribution parameters for partial parallel double-circuit transmission lines*, International Journal of Electrical Power & Energy Systems, vol. 169, 110763 (2025), DOI: 10.1016/j.ijepes.2025.110763.

[2] Wang B., Liu Y., Lu D., Yue K., Nie Y., *Unsynchronized parameter-free fault location for two or three terminal double-circuit transmission lines sharing the same tower via unscented Kalman filter*, IEEE Transactions on Power Delivery, vol. 38, no. 3, pp. 1731–1746 (2023), DOI: 10.1109/TPWRD.2022.3223410.

[3] Shen L., Yang J., *Looseness monitoring of transmission tower based on MIMU*, IEEE Sensors Journal, vol. 24, no. 2, pp. 1655–1664 (2024), DOI: 10.1109/JSEN.2023.3330228.

This paper has been accepted for publication in the AEE journal. This is the version, which has not been fully edited and content may change prior to final publication.
Citation information: DOI 10.24425/aee.2027.11175

[4] Zhu J., Wu G.N., Cao X.B., Li R.F., Shi C.Q., Gong H.K., *Electromagnetic coupling calculation and analysis of lines non-parallelly erected entirely in one common AC/DC transmission corridor*, High Voltage Engineering, vol. 40, no. 6, pp. 1724–1731 (2014), DOI: 10.13336/j.1003-6520.hve.2014.06.017.

[5] Wang S.P., Zhao D.M., Shang L.Q., Zhao X.Z., *Fault location algorithm for incomplete double-circuit transmission lines based on line segment parameters*, Transactions of China Electrotechnical Society, vol. 32, no. 20, pp. 261–270 (2017), DOI: 10.19595/j.cnki.1000-6753.tces.161202.

[6] Gao M.X., Hu Z.J., Ni S.Y., Chen J.P., Lin M.R., *Zero sequence parameter measurement of double-circuit non-full parallel transmission lines*, Power System Technology, vol. 45, no. 12, pp. 4868–4876 (2021), DOI: 10.13335/j.1000-3673.pst.2020.1936.

[7] Wang W., Li B., He J., Li B., Xie Z., Xue L., *Coupling characteristics between MMC-HVDC and AC transmission lines on the same tower and their impact on protective relaying*, International Journal of Electrical Power & Energy Systems, vol. 159, 110000 (2024), DOI: 10.1016/j.ijepes.2024.110000.

[8] Chen Y., Cao J., Wei Y., Wang X., Wang J., Fan Y., Cai L., *Analysis of induced voltage of optical fiber composite ground wire in 35 kV overhead distribution lines*, IEEE Transactions on Electromagnetic Compatibility, vol. 66, no. 1, pp. 313–323 (2024), DOI: 10.1109/TEMC.2023.3319052.

[9] Zhang W.J., Zhang G.D., Yue L.P., Zhang R., Lou P., Zhou L.L., Zhang X.Q., *Calculation and analysis on steady-state induced voltage during maintenance operation of multi parallel circuits of EHV/UHVDC/UHVAC transmission lines*, Power System Technology, vol. 38, no. 8, pp. 2310–2314 (2014), DOI: 10.13335/j.1000-3673.pst.2014.08.046.

[10] Wu G.B., Li J., Chen Y., Luo C.J., Wang R.S., Lin F., *Research on electromagnetic environment of ±800 kV and ±500 kV double-circuit DC transmission lines on the same tower*, Power System Technology, vol. 39, no. 9, pp. 2532–2538 (2015), DOI: 10.13335/j.1000-3673.pst.2015.09.024.

[11] Karami H., Mostajabi A., Azadifar M., Rubinstein M., Zhuang C., Rachidi F., *Machine learning-based lightning localization algorithm using lightning-induced voltages on transmission lines*, IEEE Transactions on Electromagnetic Compatibility, vol. 62, no. 6, pp. 2512–2519 (2020), DOI: 10.1109/TEMC.2020.2978429.

[12] Li X., He W., Tang Y., Gao S., Xie Y., Liu Y., Zhao H., *Research on the induced electric field of human under EHV AC transmission lines based on BAS-CSM algorithm*, 2023 IEEE International Conference on Power Science and Technology (ICPST), Kunming, China, IEEE, pp. 1009–1014 (2023), DOI: 10.1109/ICPST56889.2023.10165181.

[13] Lu D., Lang X.J., Yang B., Li Z.Y., Geng H., *Conductor arrangement and phase sequence optimization scheme for 500 kV four-circuit transmission lines on same tower*, Energy Engineering, vol. 120, no. 10, pp. 2287–2306 (2023), DOI: 10.32604/ee.2023.029140.

[14] Islam M.A., Jia S., Bruce N.D.B., *How much position information do convolutional neural networks encode?*, 8th International Conference on Learning Representations (ICLR), Addis Ababa, Ethiopia, pp. 1–13 (2020).

[15] Lee J., Lee Y., Kim J., Kosiorek A.R., Choi S., Teh Y.W., *Set Transformer: A framework for attention-based permutation-invariant neural networks*, 36th International Conference on Machine Learning (ICML), PMLR, vol. 97, pp. 3744–3753 (2019).

[16] Bronstein M.M., Bruna J., LeCun Y., Szlam A., Vandergheynst P., *Geometric deep learning: Going beyond Euclidean data*, IEEE Signal Processing Magazine, vol. 34, no. 4, pp. 18–42 (2017), DOI: 10.1109/MSP.2017.2693418.

[17] Xu D.G., Li Y.M., Huang S.Y., Ning L.R., Chen X., Wang C.X., Lin T., Peng Z.W., *Calculation and measurement analysis for induced voltage and current of 500 kV/220 kV mixed-voltage and four-circuit transmission lines on the same tower*, High Voltage Apparatus, vol. 61, no. 4, pp. 203−210+218 (2025), DOI: 10.13296/j.1001-1609.hva.2025.04.023.

[18] Tian W., Cao Z., *Research on induced voltage and current in deenergized line of double-circuit transmission lines on the same tower*, 2019 4th International Conference on Intelligent Green Building and Smart Grid (IGBSG), Hubei, China, IEEE, pp. 264–269 (2019), DOI: 10.1109/IGBSG.2019.8886198.

Early Access

This paper has been accepted for publication in the AEE journal. This is the version, which has not been fully edited and content may change prior to final publication.
Citation information: DOI 10.24425/aee.2027.11175

[19] Wu T., Xu X.K., Li P., Li B.L., Lyu J.F., *Multi factor analysis on induced voltage and current of 500 kV AC/DC transmission lines on the same tower*, High Voltage Apparatus, vol. 58, no. 5, pp. 47–55 (2022), DOI: 10.13296/j.1001-1609.hva.2022.05.007.

[20] Wu X., Zhang H., Karady G.G., *Transient analysis of inductive induced voltage between power line and nearby pipeline*, International Journal of Electrical Power & Energy Systems, vol. 84, pp. 47–54 (2017), DOI: 10.1016/j.ijepes.2016.04.051.

[21] Coelho L., Sotelo G., Lima A., *Detailed versus simplified representation of a pipeline for assessment of inductive and conductive couplings to an overhead transmission lines during steady-state and fault conditions*, International Journal of Electrical Power & Energy Systems, vol. 142, no. Part B, 108350 (2022), DOI: 10.1016/j.ijepes.2022.108350.

[22] Zheng Y.L., Luo R.C., Zou M., Li Z.Q., Hou J., *Induced voltage and current simulation of 380 V lineparallel operating under 330 kV double-circuit transmission lines*, Journal of Electric Power Science and Technology, vol. 36, no. 1, pp. 216–222 (2021), DOI: 10.19781/j.issn.1673-9140.2021.01.025.

[23] Li B., Dong Y., Jiao X., Chen X., Li B., Ji L., *Study on the calculation method of electrical quantity for connection line open-phase operation of wind farm connected to MMC-HVDC Considering negative sequence current suppression*, International Journal of Electrical Power & Energy Systems, vol. 159, 110056 (2024), DOI: 10.1016/j.ijepes.2024.110056.

[24] Di Bello F., Dreyer E., Ganguly S., Gross E., Heinrich L., Ivina A., Tusoni M., *Reconstructing particles in jets using set transformer and hypergraph prediction networks*, The European Physical Journal C, vol. 83, 596 (2023), DOI:10.1140/epjc/s10052-023-11677-7.

[25] He C., Li R., Li S., Zhang L., *Voxel set transformer: a set-to-set approach to 3D object detection from point clouds*, 2022 IEEE/CVF Conference on Computer Vision and Pattern Recognition (CVPR), New Orleans, LA, USA, pp. 8417–8427 (2022).

[26] Collenne J., Iguernaissi R., Dubuisson S., Merad D., *Reset: aresidual set-transformer approach to tackle the ugly-duckling sign in melanoma detection*, 2024 IEEE International Conference on Image Processing (ICIP), Abu Dhabi, United Arab Emirates, IEEE, pp. 3186–3191 (2024), DOI: 10.1109/ICIP51287.2024.10647287.

Early Access